Peptide-siRNA nanocomplexes targeting NF-κB subunit p65 suppress nascent experimental arthritis

Hui-fang Zhou,[1] Huimin Yan,[1] Hua Pan,[2] Kirk K. Hou,[2] Antonina Akk,[1] Luke E. Springer,[1] Ying Hu,[1] J. Stacy Allen,[2] Samuel A. Wickline,[2] and Christine T.N. Pham[1]

[1]Division of Rheumatology and [2]Division of Cardiology, Department of Medicine, Washington University School of Medicine, Saint Louis, Missouri, USA.

The NF-κB signaling pathway is implicated in various inflammatory diseases, including rheumatoid arthritis (RA); therefore, inhibition of this pathway has the potential to ameliorate an array of inflammatory diseases. Given that NF-κB signaling is critical for many immune cell functions, systemic blockade of this pathway may lead to detrimental side effects. siRNAs coupled with a safe and effective delivery nanoplatform may afford the specificity lacking in systemic administration of small-molecule inhibitors. Here we demonstrated that a melittin-derived cationic amphipathic peptide combined with siRNA targeting the p65 subunit of NF-κB (p5RHH-p65) noncovalently self-assemble into stable nanocomplexes that home to the inflamed joints in a murine model of RA. Specifically, administration of p5RHH-p65 siRNA nanocomplexes abrogated inflammatory cytokine expression and cellular influx into the joints, protected against bone erosions, and preserved cartilage integrity. The p5RHH-p65 siRNA nanocomplexes potently suppressed early inflammatory arthritis without affecting p65 expression in off-target organs or eliciting a humoral response after serial injections. These data suggest that this self-assembling, largely nontoxic platform may have broad utility for the specific delivery of siRNA to target and limit inflammatory processes for the treatment of a variety of diseases.

Introduction

The NF-κB family consists of 5 members: RelA (also known as p65), Rel (also known as c-Rel), RelB, p105 (processed to p50), and p100 (processed to p52) (1). These members form homo- and heterodimers that, in the resting cell, are normally held inactive in the cytoplasm by association with inhibitors, the IκB proteins. Activation of NF-κB is controlled by the IκB kinase (IKK) complex that phosphorylates IκB proteins and targets them for degradation, releasing the NF-κB subunits for nuclear translocation and transactivation of a multitude of responsive genes, including several inflammatory cytokines. Thus, the NF-κB pathway plays a crucial role in the inflammatory response of macrophages and lymphocytes in many inflammatory diseases.

Rheumatoid arthritis (RA) is a chronic and debilitating inflammatory arthropathy. Although the etiology of RA remains controversial, the hallmark of the disease is characterized by inflammation of the synovial lining of diarthrodial joints, massive synovial proliferation, and an influx of inflammatory cells, macrophages, and lymphocytes through leaky angiogenic blood vessels (2–4). This cellular influx and synovial proliferation lead to the release of inflammatory cytokines and matrix-degrading enzymes, all of which contribute to the destruction of connective tissue, cartilage, and subchondral bone of the affected joints. Activated macrophages and lymphocytes are thus considered principal targets for therapy in RA. Recent understanding of inflammatory responses in RA has led to the development of several effective treatment modalities. These include a number of "biologics" aimed at inhibiting the action of several inflammatory cytokines, including IL-1β, IL-6, and TNF-α (5). Yet despite these advances, many patients with RA fail to respond to these new biologic agents. Moreover, studies have shown that around half of the initial responders eventually stop responding in the first year due to inefficacy or have to stop therapy altogether due to side effects (6). Although other biologic therapies, such as the JAK kinase inhibitor tofacitinib, are beginning to emerge (7), the complexity of RA, the heterogeneity of patients, and previous experience with biologics suggest that targeting a single receptor or cytokine pathway will not lead to a predictable response in patients.

We reasoned that the simultaneous interruption of several inflammatory cytokine pathways would lead to a higher likelihood of abrogating disease progression and promoting disease remission. The role of NF-κB in inflammation in general and RA in particular as a central checkpoint is well established (8–11). Accordingly, in the present work, we sought to define the utility of a novel siRNA delivery approach using nanoparticles targeted to the NF-κB signaling subunit p65, which is a principal transcriptional regulator of the canonical NF-κB pathway (12). The nanoparticle construct is composed of a self-assembling peptide-siRNA complex that serves to protect the siRNA from serum deactivation, while avoiding reticuloendothelial system uptake and delivering functional oligonucleotides to selected inflammatory targets (13, 14). Key features of the complex that promote sequentially coordinated endosomal uptake, endosomal lysis, and siRNA release depend on specific molecular features of the carrier peptide (13), which is derived through modification of the bee venom peptide melittin (15). Selected amino acid truncations and substitu-

Authorship note: Hui-fang Zhou, Huimin Yan, and Hua Pan contributed equally to this work.
Conflict of interest: The authors have declared that no conflict of interest exists.
Submitted: February 13, 2014; **Accepted:** July 3, 2014.
Reference information: *J Clin Invest*. 2014;124(10):4363–4374. doi:10.1172/JCI75673.

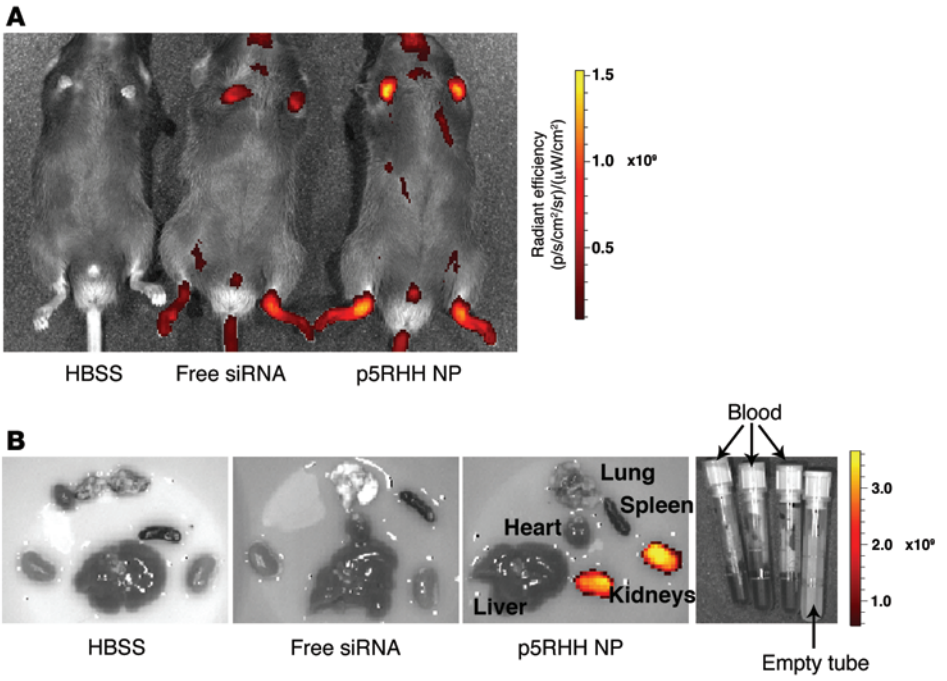

Figure 1. p5RHH siRNA nanoparticles accumulate in inflamed paws. Day 4 arthritic mice received i.v. injection of HBSS, free Cy5.5-labeled scrambled siRNA (Free siRNA), p5RHH-Cy5.5–labeled scrambled siRNA nanoparticles (p5RHH NP), and in vivo fluorescent images were acquired over time. (**A**) Fluorescent signals were readily detected in the inflamed paws of arthritic mice injected with free Cy5.5 siRNA and p5RHH siRNA nanoparticles, but not HBSS. Note the substantially higher level of fluorescence in the p5RHH siRNA nanoparticle–injected animal at 7 hours. (**B**) Organs and blood were collected 2 hours after injection for fluorescence imaging. The highest signals were detected mainly in kidneys, while uptake in the reticuloendothelial system (liver and spleen) was markedly lower. Note that p5RHH siRNA nanoparticles were largely cleared from the circulatory system (blood) 2 hours after injection (far right). Pseudocolor "efficiency image" was used to illustrate the organ accumulation of Cy5.5-labeled siRNA.

tions mitigate the undesirable pore-forming capacity of peptide, yet retain its ability to condense siRNA and facilitate endosomal escape, as previously reported (13, 16). A simple mixing procedure of only 10 minutes yields a complex that is small enough (~55 nm) to passively diffuse rapidly into inflamed tissues, where it is retained, yet avoids hepatic sequestration (14). Using a mouse model of antibody-mediated inflammatory arthritis, we found that anti–NF-κB peptide-siRNA self-assembling nanocomplexes (13, 14) effectively silenced the expression of p65 as well as a broad array of downstream cytokine effectors in the inflamed paws, and also suppressed arthritis with minimal off-target molecular effects.

Results

p5RHH siRNA nanocomplexes localize to the inflamed joints. Collagen-induced arthritis (CIA) in mice is an experimental arthritis model that in many ways resembles RA. Immunization of susceptible strains of mice with chick or bovine type II collagen (CII) leads to the development of anti-CII antibodies that initiate polyarticular arthritis (17, 18). Transfer of a combination of anti-CII monoclonal antibodies derived from mice with CIA also leads to a severe arthritis accompanied by bone erosion and cartilage destruction (19). In this CII antibody–induced arthritis (CAIA) model, we injected 6- to 8-week-old male DBA1/J mice i.p. on day 0 with a cocktail of 5 monoclonal anti-CII antibodies (1.5 mg), followed by i.p. injection with LPS (50 μg) on day 3. Arthritis was evident consistently within 24 hours after LPS injection and persisted for 2–3 weeks. We administered HBSS, free Cy5.5-labeled scrambled siRNA or p5RHH-Cy5.5–labeled scrambled siRNA nanocomplexes (referred to herein as p5RHH siRNA nanoparticles) to arthritic mice on day 4 and followed particle accumulation in vivo after injection through whole-body fluorescence imaging (IVIS). Free Cy5.5-labeled scrambled siRNA and p5RHH siRNA nanoparticles both localized to the inflamed joints. However, we detected a substantially higher level of Cy5.5 fluorescence in the mouse injected with p5RHH siRNA nanoparticles (Figure 1A). The signal remained stable for at least 7 hours after injection, with gradual decay over time (Supplemental Figure 1; supplemental material available online with this article; doi:10.1172/JCI75673DS1).

While previous studies have shown that i.v. administered free siRNAs are cleared from the system within 15 minutes (20), we found here that Cy5.5-labeled siRNA packaged in the p5RHH siRNA nanocomplexes were readily detected in the kidneys 2 hours after injection, and the signals persisted up to 24 hours (Figure 1B and Supplemental Figure 2), which suggests that siRNAs packaged in non-albumin-coated nanoparticles had a different clearance kinetics than free siRNA. In contrast, the spleen and liver — traditional clearance organs for many types of nanoparticles — did not sequester substantial amounts of particles (Figure 1B). Furthermore, we observed no signal from Cy5.5-labeled free siRNA in any organ 2 hours after i.v. administration of an equivalent load (Figure 1B), corroborating the rapid clearance and instability of free siRNA compared with the more stable nanoparticle-formulated siRNA.

Because we detected no significant fluorescent signals associated with peripheral blood or splenic phagocytes (monocytes/macrophages and neutrophils) after p5RHH siRNA nanoparticle injection (Supplemental Figures 3–6), it is likely that accumulation of nanoparticles represents direct delivery into the joint milieu without peripheral monocyte or splenic macrophage uptake and subsequent recruitment to the site of inflammation. To further explore this hypothesis, we injected day 6 arthritic mice with free Cy3-labeled p65 siRNA or Cy3-labeled p5RHH-p65 siRNA nanocomplexes and examined synovial tissues for intracellular particle accumulation. At 2.5 hours after injection, we observed a number of tissue macrophages, in the immediate vicinity of blood vessels, that harbored high intracellular levels of the p5RHH-p65 siRNA nanoparticles (Figure 2). In contrast, scant intracellular Cy3 signal was visible in paw sections of the animal injected with free p65 siRNA.

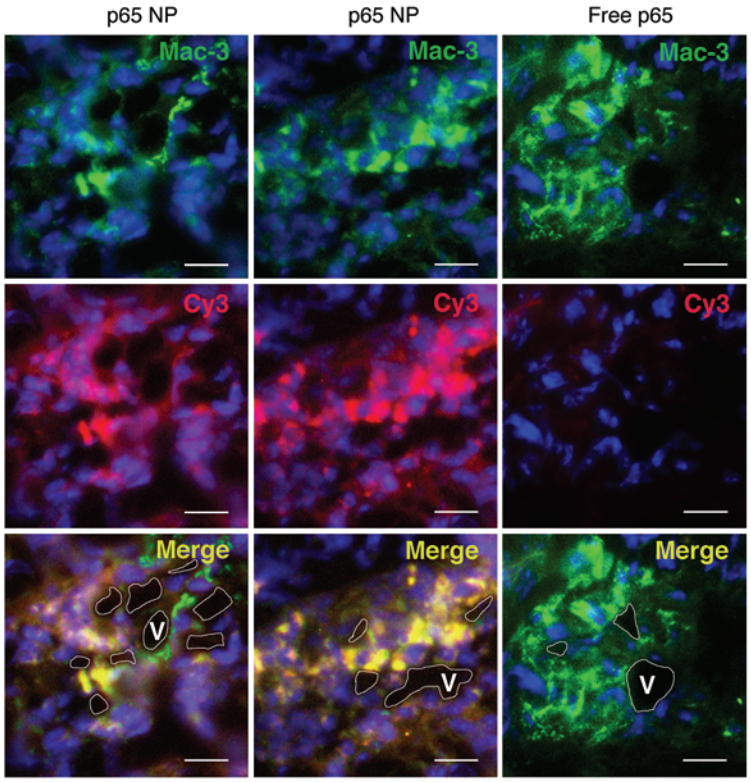

Figure 2. p5RHH siRNA nanoparticles target synovial macrophages. Day 6 arthritic mice were injected with p5RHH-Cy3–labeled p5RHH-p65 siRNA nanoparticles (p65 NP) or free Cy3-labeled p65 siRNA (free p65). At 2.5 hours, mice were sacrificed and paws obtained for immunofluorescence study. In the mouse injected with p5RHH-p65 siRNA nanoparticles, Cy3 signal (red) colocalized (yellow in merged images) with synovial macrophages (Mac-3+, green). In contrast, only very low signal was detected in the synovial macrophages of the mouse injected with free p65 siRNA. DAPI (blue) stained nuclei. Some blood vessels (V) are outlined in white. Scale bar: 20 μm.

p5RHH-p65 siRNA nanocomplexes suppress CAIA. CAIA was induced as above, and on day 4 (24 hours after LPS injection), when early arthritis was established in all mice, animals were randomly divided into 3 treatment groups: HBSS control, p5RHH siRNA complexes, and p5RHH-p65 siRNA nanocomplexes. Nanoparticles were administered i.v. serially on days 4, 5, and 6. Ankle thickness changes, arthritis score, and percent weight loss were assessed over a period of 10 days. p5RHH-p65 siRNA nanoparticle treatment rapidly stabilized ankle swelling and significantly suppressed arthritis score, an effect that persisted until at least day 10 (Figure 3, A–C). Administration of p5RHH siRNA nanocomplexes did not significantly alter arthritis progression compared with HBSS treatment (Figure 3, A–C). In addition, treatment with p5RHH-p65 siRNA nanoparticles did not adversely affect the animals' weight loss beyond that induced by inflammation and LPS injection (Figure 3D). On day 10, mice that received p5RHH-p65 siRNA nanoparticles showed an approximately 75% reduction in ankle thickness and 65% reduction in arthritis score compared with HBSS and p5RHH siRNA controls. Histologic examination of paws harvested on day 10 revealed that treatment with p5RHH-p65 siRNA nanoparticles significantly attenuated the influx of leukocytes to the inflamed paws, protected against bone erosion, and preserved cartilage integrity (Figure 3, E–H). On the other hand, we observed no histologic difference between animals treated with p5RHH siRNA nanoparticles and those injected with HBSS (Figure 3, E–H). Furthermore, administration of equivalent doses of free p65 siRNA did not alter arthritis progression or production of joint-associated inflammatory cytokines (TNF-α, IL-1β, IL-6, and MCP-1) compared with HBSS injection (Figure 4, A and B). These results confirmed the superiority of the p5RHH-based platform in delivering p65 siRNA to synovial macrophages and suppressing their inflammatory responses. While free p65 siRNA also diffused into inflamed tissues, the low level of intracellular accumulation was insufficient to suppress p65 expression (Figure 4C).

In parallel with improved clinical indices and histology, we found that joint-associated inflammatory cytokine production was significantly suppressed in mice treated with p5RHH-p65 siRNA nanoparticles (Figure 5A). In addition, mRNA and protein expression levels of p65 were specifically downmodulated in the paws of these animals, while those of related NF-κB family members (p100, p105, and RelB) were preserved (Figure 5, B and C). Moreover, we confirmed that p65 expression in synovial macrophages was decreased at the single-cell level (Figure 5D), thus corroborating the findings above that p5RHH-p65 siRNA nanocomplexes targeted macrophages and suppressed NF-κB–dependent inflammatory response in the mitigation of clinical arthritis. In contrast, protein levels of p65 and other NF-κB family members in off-target organs such as liver, spleen, brain, and kidneys were all relatively preserved (Figure 6). Taken together, these findings provide proof of concept that p5RHH siRNA nanoparticles targeting the NF-κB p65 subunit selectively silenced the gene expression in the intended organs (joints/synovium) and potently suppressed ongoing inflammation in a robust model of acute inflammatory arthropathy.

In vivo toxicity profile of p5RHH-p65 siRNA nanocomplexes. To examine the safety of p5RHH-p65 siRNA nanoparticles in vivo, we first determined their effect on hematologic parameters. Serial i.v. injections of p5RHH-p65 siRNA nanoparticles did not affect peripheral wbc counts and differentials, hemoglobin levels, or platelet counts (Figure 7A). Although the relatively high accumulation of nanoparticles in the kidney (Figure 1B and ref. 14) was suggestive of preferential renal clearance, we observed no deleterious effects on renal function, as reflected by normal electrolytes and levels of blood urea nitrogen and creatinine (Figure 7, B and C). Finally, we detected no changes among treatment groups in liver function tests (Figure 7D). These results point to a favorable toxicity profile in vivo after multiple doses.

Effects of p5RHH-p65 siRNA nanocomplexes on immune responses. Next we examined the effects of p5RHH-p65 siRNA nanoparticles on immune cell function in nontarget organs. On day 10, spleens from different treatment groups were harvested, and splenocytes/splenocyte subpopulations were enumerated. We noted a trend toward higher numbers of total splenocytes in the p5RHH-p65 siRNA nanoparticle treatment group, perhaps reflecting less

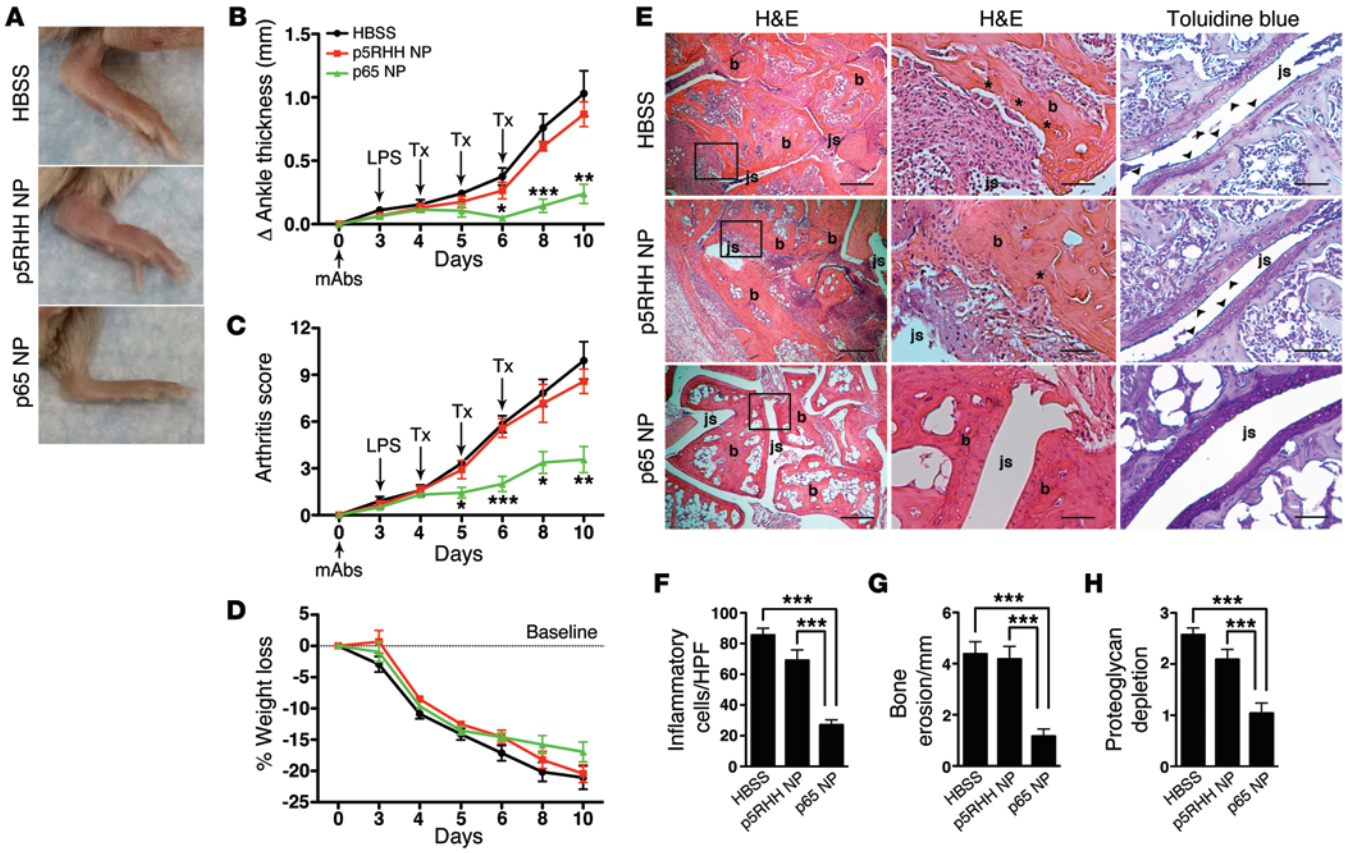

Figure 3. p5RHH-p65 siRNA nanotherapy suppresses inflammation in CAIA. CAIA arthritis was induced as detailed in Methods (day 3 LPS injection is indicated). On day 4, mice were randomly divided into 3 treatment groups: HBSS, p5RHH siRNA nanoparticles, and p5RHH-p65 siRNA nanoparticles. Nanoparticles or HBSS were administered i.v. serially on days 4, 5, and 6 (Tx). (**A**) Representative photographs of day 10 paws from the 3 treatment groups. (**B**–**D**) Change in ankle thickness (**B**), arthritis score (**C**), and percent weight loss (**D**) were chronicled over time. Values are mean ± SEM (n = 6–8 per group). (**E**) Day 10 paws were harvested, sectioned, and stained with H&E to evaluate for the number of inflammatory cells/erosions and toluidine blue to evaluate for cartilage integrity. Note the intense inflammatory infiltrates in and surrounding the joint space in HBSS- and p5RHH siRNA–treated animals while joint space in p5RHH-p65 siRNA–treated animals was largely devoid of cellular infiltrates (left). In higher-power images, erosions (asterisks) were noted along the bone surface in HBSS- and p5RHH siRNA–treated animals (middle). Extensive proteoglycan depletion (arrowheads) was also noted in HBSS- and p5RHH siRNA–treated animals (right). b, bone; js, joint space. Scale bars: 400 μm (left), 100 μm (middle), 50 μm (right). (**F**–**H**) Inflammatory infiltrates per high-power field (HPF; **F**), erosions (**G**), and degree of proteoglycan depletion (**H**) were quantified as detailed in Methods. *P < 0.05, **P < 0.01, ***P < 0.001.

cellular efflux from spleen to inflamed sites (joints); however, this difference did not reach statistical significance (Figure 8A). We also observed no difference in the composition of the major splenocyte subpopulations, including $CD4^+$ and $CD8^+$ T cells, $CD19^+$ B cells, $NK1.1^+$ natural killer cells, and $Foxp3^+$ T regulatory cells (Figure 8B). To further assess immune cell function after p5RHH-p65 siRNA nanoparticle treatment, we isolated splenic $CD4^+$ T cells and stimulated them ex vivo on plate-bound anti-CD3 monoclonal antibody. Anti-CD3–activated $CD4^+$ T cells from different treatment groups proliferated equivalently and released similar amounts of cytokines (TNF-α, IFN-γ, IL-6, and IL-10; Figure 8, C–F, and Supplemental Figure 7).

We previously observed that injection of certain types of functionalized nanoparticles can elicit swift complement activation, the intensity of which depends on the specific type of nanoparticle surface functionalization (21, 22). To assess whether the interaction of peptide-siRNA nanoparticle complexes with the host complement system could lead to robust activation, we injected mice with HBSS, p5RHH siRNA nanoparticles, or p5RHH-p65 siRNA nanoparticles and collected their plasma at 30 minutes to quantify the C3 degradation product C3a as evidence of in vivo complement activation (22). We observed an increase in C3a levels in mice injected with p5RHH-p65 siRNA nanoparticles compared with HBSS-injected animals, whereas injection with perfluorocarbon nanoparticles functionalized with 50 molar percentage of N-[1-(2,3-dioleoyloxy) propyl]-N,N,N-trimethylammonium methyl-sulfate (DOTAP; ref. 22) generated markedly higher levels of C3a (Figure 9A).

To address the potential immunogenicity of p5RHH siRNA nanoparticles, we measured specific antibody responses against both p5RHH peptide and p5RHH siRNA nanocomplexes after 3 serial injections on days 4, 5, and 6. Sera were collected from treated animals on day 10, and IgM and IgG antibodies specific for the peptide or the nanocomplex were measured by ELISA-based assay on microtiter plates coated with p5RHH siRNA nanoparticles or p5RHH-p65 siRNA nanoparticles. No significant difference was observed among the 3 treatment groups for IgM or IgG responses (Figure 9, B and C). We also measured total antibody levels in the treated animals and observed no elevation in total IgM or IgG

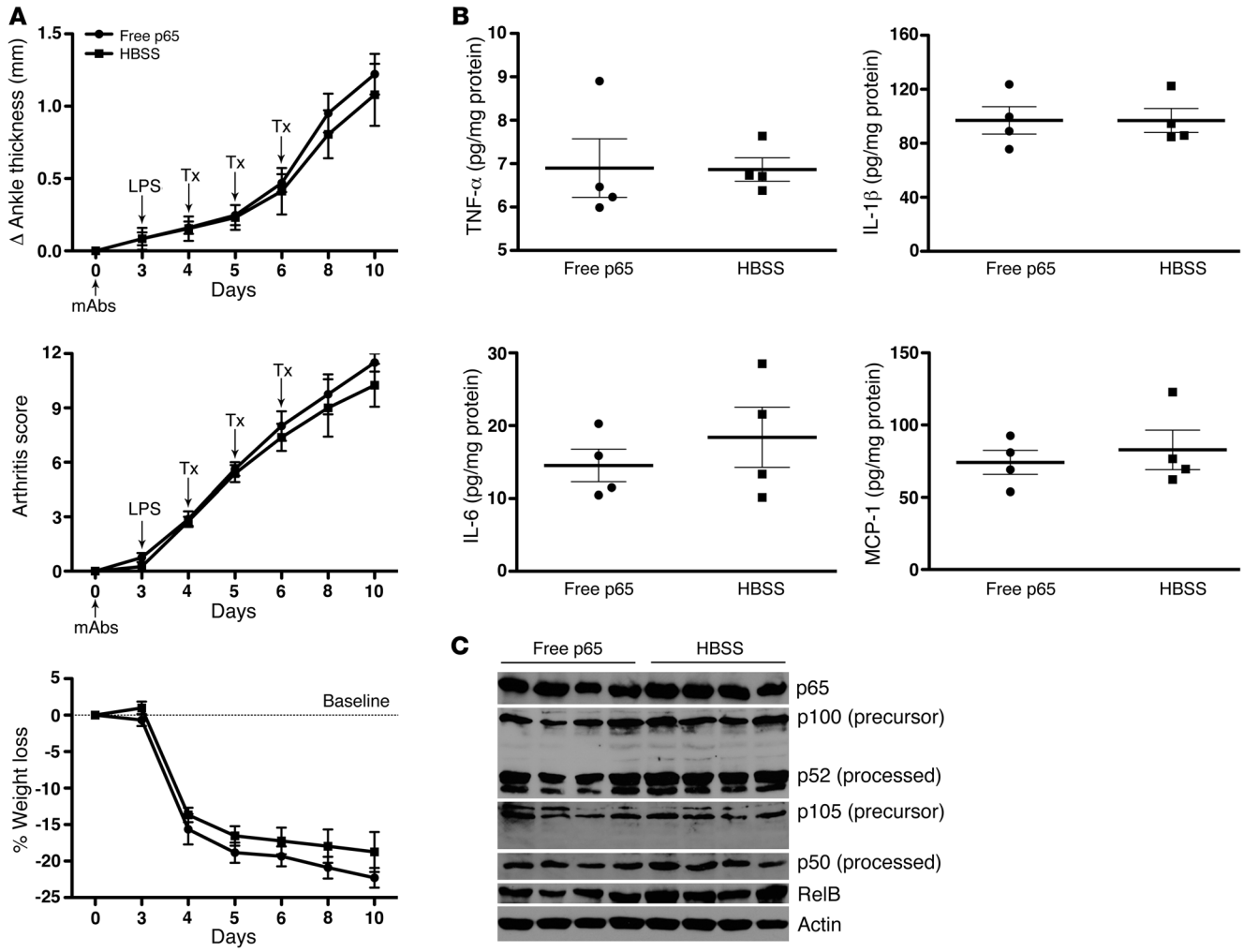

Figure 4. Administration of free p65 siRNA does not suppress CAIA. Arthritis was induced as detailed in Methods (day 3 LPS injection is indicated). On day 4, mice were randomly divided into 2 treatment groups: HBSS and free p65 siRNA. Treatment (Tx) was administered i.v. serially on days 4, 5, and 6. (**A**) Changes in ankle thickness, arthritis score, and percent weight loss were chronicled over time. On day 10, animals were sacrificed and paws processed for (**B**) cytokine levels and (**C**) Western blot analysis of p65 and related NF-κB family members (p100, p105, and RelB). p100 and p105 were detected in both precursor and processed forms (p52 and p50, respectively). No statistical difference between treatments was noted.

levels (Figure 9D). These results suggest that, at the administered dose and injection schedule, these p5RHH-based nanoparticles did not elicit systemic adaptive immune responses.

Discussion

Here, we demonstrated that the melittin-derived p5RHH peptides complexed with anti-p65 siRNA successfully and potently suppress ongoing experimental arthritis. Evidence gathered from genetic knockout mice suggests a central role for NF-κB, in particular the classical or canonical pathway controlled by p65 or p50, in RA and other inflammation-related pathologies (1, 8). Because activation of the canonical pathway results in the transactivation of a number of inflammatory mediators, including TNF-α, chemokines, and matrix metalloproteases, NF-κB subunit p65 represents an attractive target in RA, especially in instances in which inhibition of single cytokines proves ineffective. Despite much interest, small-molecule inhibitor approaches have not been promising due to lack of specificity (23). Alternatively, gene silencing might be expected to achieve the specificity that is lacking in small-molecule inhibitors. When coupled with a safe and effective delivery nanoplatform, this genetic approach may circumvent some of the shortcomings of small-molecule inhibitors by specifically suppressing inflammation in the joints, while largely sparing off-target toxicities.

siRNA-based therapeutics for the treatment of inflammatory diseases have received increasing attention of late. Several clinical trials are ongoing for various diseases, including age-related macular degeneration, viral infections, respiratory disorders, and cancer (reviewed in ref. 24). However, the potential use of siRNA therapy in RA has not progressed beyond the preclinical models. These studies range from local electroporation to deliver siRNA directly into joint tissue of arthritic mice to several studies of systemic delivery of liposome- or polymer-based nanoparticles delivering anti-cytokine or anti-cytokine receptor siRNA (25–30). Although these preclinical studies all showed efficacy, potential off-target effects and immune responses were rarely fully addressed.

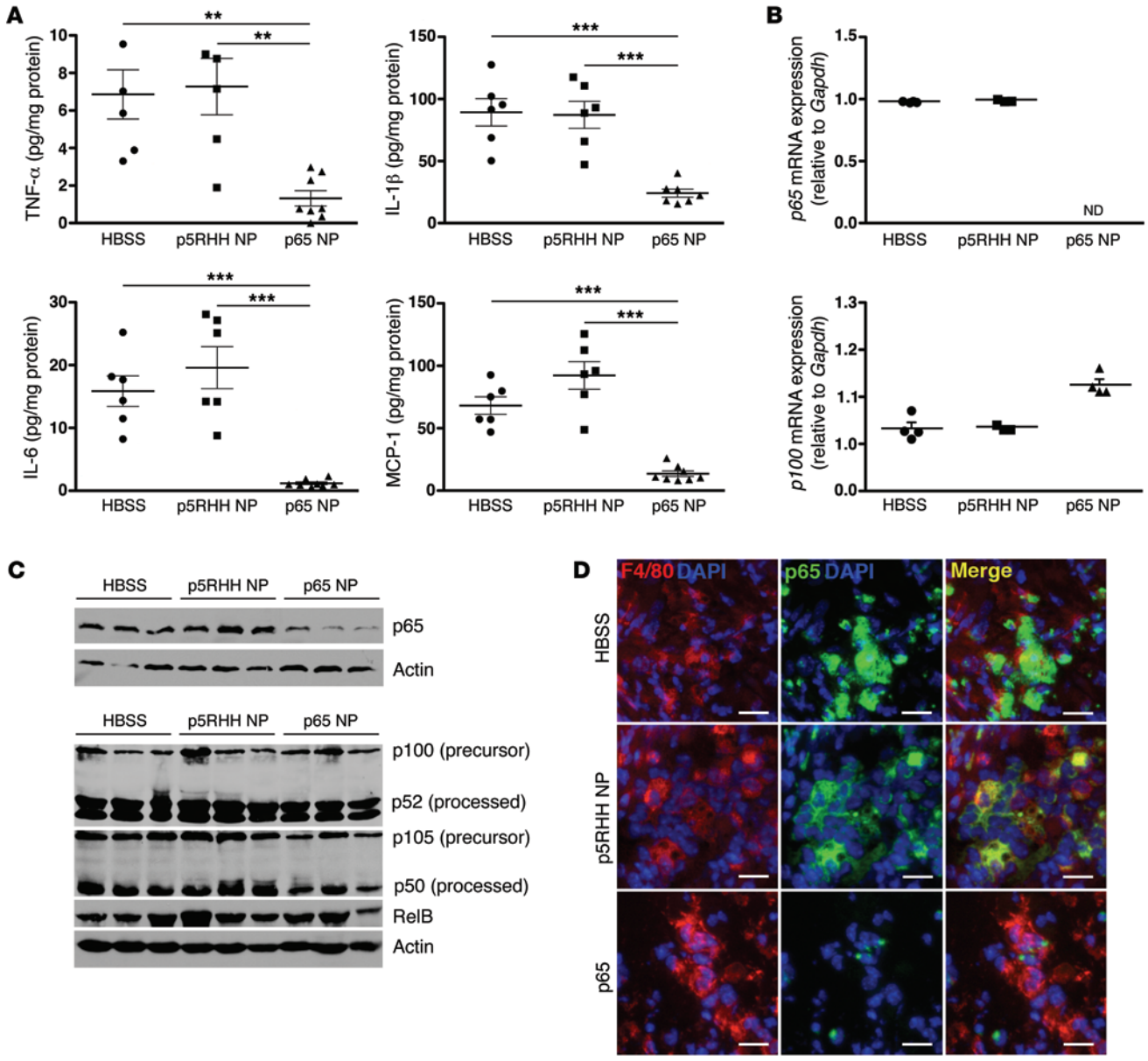

Figure 5. p5RHH-p65 siRNA nanoparticles downmodulate inflammatory cytokine production and the expression of p65 specifically in the joints. (**A**) Day 10 paws were homogenized, and cleared lysates were assayed for inflammatory cytokines. $^{**}P < 0.01$, $^{***}P < 0.001$. (**B**) Paws were processed and examined for *p65* and *p100* mRNA expression relative to *Gapdh* by real-time PCR. ND, not detected. (**C**) Paw lysates were probed for the presence of p65, p100, p105, and RelB by Western blotting. The protein expression of p65 was attenuated in the paw lysates of p5RHH-p65 siRNA nanoparticle–treated animals, whereas expression of related NF-κB family members was relatively preserved. The analysis was repeated with a second cohort of mice treated with the same regimen, and similar results were obtained. (**D**) Day 10 paw sections were probed for macrophages (F4/80$^+$; red) and p65 (green). DAPI (blue) stained nuclei. Note that p65 protein expression per single cell was decreased in the mouse treated with p5RHH-p65 siRNA nanoparticles. Scale bar: 25 μm.

Cationic lipids and polymers have been successfully used for in vivo siRNA delivery in preclinical models; however, potential toxicities (31–33) have hindered the clinical translation of these platforms. Moreover, these agents tend to aggregate with serum proteins in vivo and often mediate robust complement activation with potential deleterious effects (34–36). We recently reported the development of an amphipathic peptide-based siRNA nanoplatform (13, 14) that uses a modified version of the bee venom component melittin to transport siRNA (15). Melittin is a well-studied peptide with pore-forming features that derive from its ability to insert into lipid membranes stably through hydrophobic interactions among resident membrane phospholipids interacting with its α-helical peptide secondary structure (16, 37, 38). Subsequent multimeric oligomerization establishes a membrane pore, resulting in disruption and cell death. Alternatively, apoptosis may be induced through interactions with intracellular mitochondrial membranes, depending on membrane cholesterol content (39, 40).

In order to limit the immediate pore-forming potential of melittin, we initially modified its sequence by selective truncations to produce a shorter amphipathic cationic peptide (termed

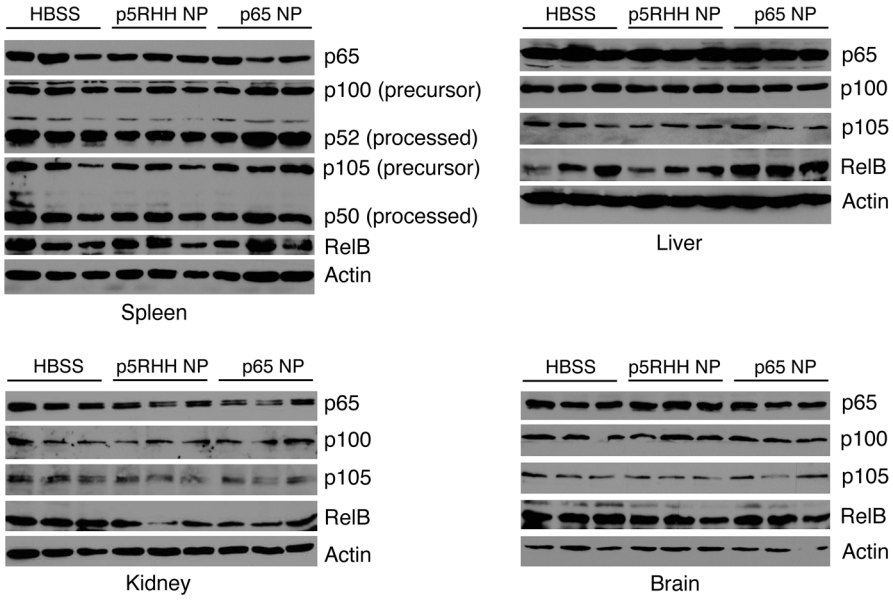

Figure 6. p65 downmodulation is specific to the inflamed joints. Arthritic mice were serially treated with HBSS, p5RHH siRNA nanoparticles, or p5RHH-p65 siRNA nanoparticles on days 4, 5, and 6. Day 10 off-target organs (spleen, liver, kidney, and brain) were processed, and protein lysates were probed for expression of p65 and related NF-κB family members (p100, p105, and RelB) by Western blotting. The processed forms of p100 and p105 (p52 and p50, respectively) were only detected in spleen.

p5) that serves well as a "cargo carrier" capable of inserting rapidly into lipid membranes, but is substantially less lytic compared with native melittin (5,700% decrease; ref. 38). After uptake of the nanoparticles into endosomes, the residual lytic activity of the p5 peptide enables the disruption of endosomal membrane, allowing the siRNA to escape, as previously shown (14). Further modifications of the peptide sequence were shown to enable numerous other useful attributes, such as protected siRNA transport in circulation and rapid delivery to target tissues through passive permeation in addition to endosomal escape after pinocytotic uptake and concomitant rapid release of siRNA that depends on endosomal acidification and peptide protonation (13, 14). Avoidance of liver/spleen sequestration and renal clearance also serve to promote more focused tissue interactions, particularly under conditions of inflammation and enhanced vascular permeability, as in cancers (14). Finally, the approach is agnostic as to the exact oligonucleotide sequence, and the entire complex can be formed within as little as 10 minutes by a simple mixing procedure that allows noncovalent self assembly of cationic and anionic moieties into ~55-nm particles ready for direct injection.

The safety of the system in these short-term applications at least appears promising for translation, based on the extensive set of studies we conducted to rule out organ, tissue, and biochemical off-target effects. Initial studies suggested that 3 serial injections of the nanocomplexes did not elicit a specific humoral response. However, immunogenicity after repeated dosings of the nanocomplexes will require further evaluation. These observations also point to a lack of knockdown of normal levels of p65 in other tissues, in which physiological functioning of NF-κB would be expected to remain undisturbed, including innate and adaptive T cell–mediated immune responsiveness. The rapid entry into desired tissue compartments and subsequent prolonged sequestration may initiate through inflamed and leaky vasculature, much like the endothelial permeability and retention (EPR) effect proposed for nanoparticle cancer localization.

In concert with primary kidney clearance, and given the advantageous particle sizes for the complex, the potential for permeation into other normal tissues appears to be minimized. The avoidance of liver and spleen sequestration and the ability to maintain normal immune responsiveness elsewhere is a particular advantage of this technology, in contrast to other systems that might impair immune reactivity (41), with potentially deleterious consequences for cancer surveillance and susceptibility to infectious diseases. We speculate that the lack of liver/spleen uptake for these types of nanoparticles may be related to their immediate acquisition of an albumin coating after injection, which might be anticipated for any nanosystem in the circulation. Indeed, albumin is known to act both as a particle-stabilizing agent and as a dysopsonin, thereby avoiding liver sequestration (14). Moreover, we have shown previously that an exogenous albumin coating enhances transfection potential in vitro, which may offer another advantage for the system after interacting with serum proteins in vivo (13).

In summary, we have shown that the p5RHH siRNA platform is a potent and facile delivery system due to its self-assembling property. The ease with which the siRNA moiety can be switched out, because it is not chemically conjugated, suggests that its utility can be extended to a number of therapeutic RNA candidates. In addition to therapeutic applications, the platform may also be used to interrogate pathway involvement in the pathogenesis of RA and other inflammatory diseases. Although we took advantage of the EPR effect to deliver the nanocomplexes in this study, targeting ligands could be added for enhanced local accumulation or cell interactions if the need arises. Finally, it is important to point out that the nanoparticle formulation is critical to the success of the agent, because even though free siRNA localizes to the intended site (inflamed joints), it exhibits no gene silencing activity. This is likely because siRNA packaged as p5RHH nanocomplexes gained access to the cell cytoplasm through micropinocytosis (14), while the free siRNA could not. Taken together, our results suggest that this platform, with its relative site-specific gene silencing activity combined with minimal off-target toxicities, may have real translational potential for the treatment of many inflammatory processes beyond arthritis.

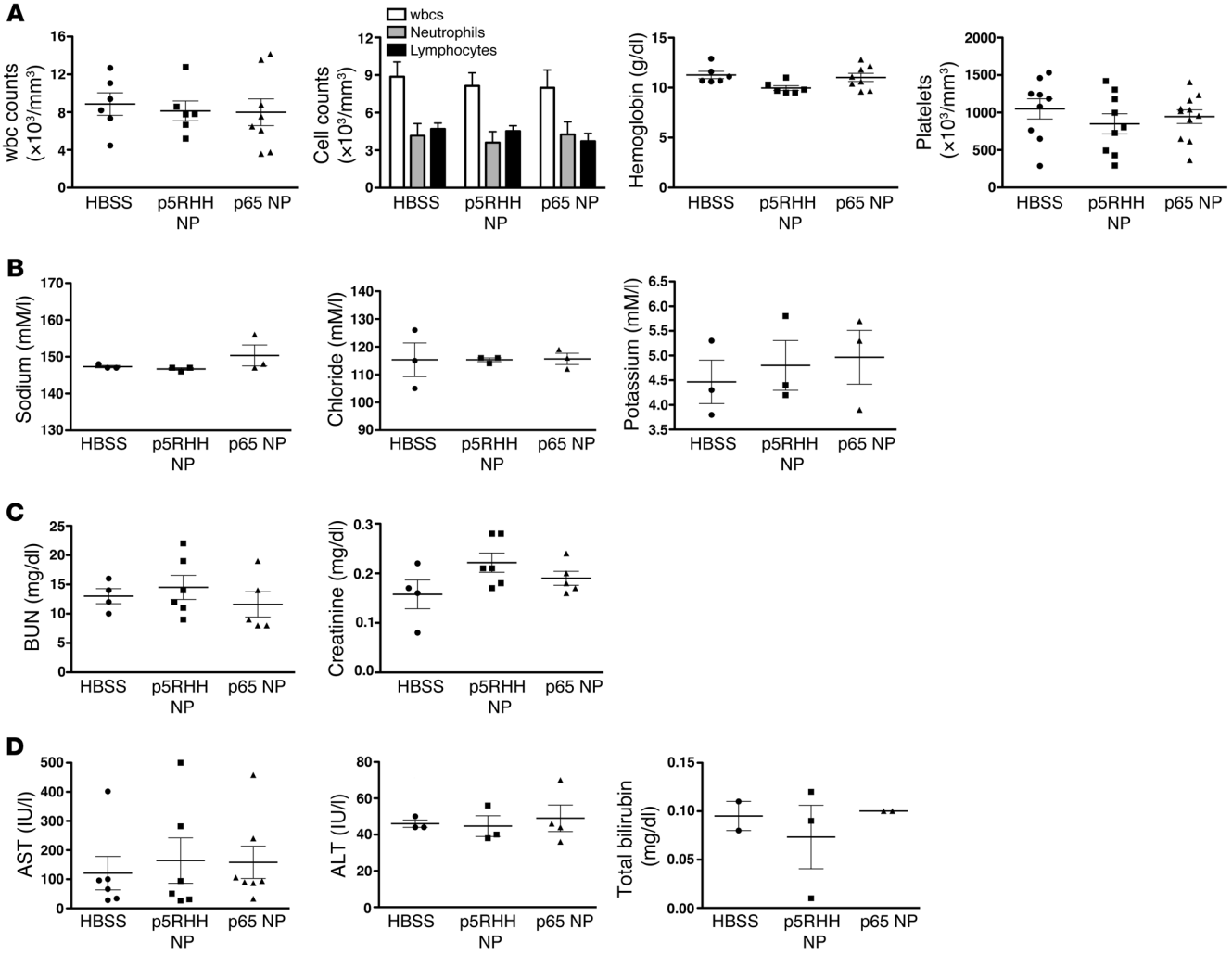

Figure 7. In vivo toxicity profile of p5RHH-p65 siRNA nanoparticles. Arthritic mice were serially treated with HBSS, p5RHH siRNA nanoparticles, or p5RHH-p65 siRNA nanoparticles, on days 4, 5, and 6, and blood was obtained on day 10. (**A**) Hematologic parameters: wbc counts/differentials, hemoglobin, and platelet counts. (**B**) Serum electrolytes: sodium, chloride, and potassium. (**C** and **D**) Renal (**C**) and liver (**D**) function. BUN, blood urea nitrogen. There was no significant difference noted among the 3 treatment groups.

Methods

Preparation of p5RHH siRNA nanocomplexes. p5RHH peptide (provided by Genscript) was dissolved at 10 mM in DNAse-, RNAse-, and protease-free sterile purified water (Cellgro) and stored in 10-μl aliquots at –80°C before use. The Cy5.5-labeled scrambled siRNAs and Cy3-labeled p65 siRNAs were ordered from Sigma-Aldrich, dissolved at 100 μM in 1× siRNA buffer (Thermo Scientific), and stored in 10-μl aliquots at –80°C before use. The p5RHH siRNA nanoparticles were prepared by mixing equal volumes of the aforementioned p5RHH peptide and siRNA at a peptide/siRNA ratio of 1:20 in HBSS with Ca^{2+} and Mg^{2+} (Gibco, Life Technologies) and incubated on ice for 10 minutes before injection (14). This preparation typically results in a nominal nanoparticle size of approximately 55 nm after applying a stabilizing albumin coating, as measured by atomic force microscopy (14), and zeta potentials varying from +12 to –5.5 mV and polydispersity index varying from 0.120 to 0.190 depending on size and the presence or absence of an exogenously applied albumin coating (13). We also have previously shown that the uncoated particles are slightly smaller (by 14%) than the albumin-coated particles by dynamic light scattering after 40 minutes of mixing the components (13).

Arthritis induction and treatment. All mice were kept in a pathogen-free condition at Washington University Specialized Research Facility. Arthritis was induced using the collagen antibody–induced arthritis model (CAIA) with Arthrogen-CIA arthrogenic monoclonal antibody 5-clone cocktail (Chondrex). 6- to 8-week-old male DBA/1J mice (Taconic) were injected i.p. with 1.5 mg of the 5-clone antibody cocktail on day 0 and 50 μg of LPS on day 3. Starting on day 4, when early arthritis was established, animals received daily serial i.v. injections of p5RHH siRNA nanoparticles, p5RHH-p65 siRNA nanoparticles (1 mg/kg i.v. by tail vein), or an equivalent concentration of free p65 siRNA for 3 consecutive days. HBSS injection served as the control. Clinical manifestations of arthritis were assessed daily on a scale of 0–3 (0, no swelling or erythema; 1, slight swelling or erythema; 2, moderate erythema and swelling in multiple digits or entire paw; 3, pronounced erythema and swelling of entire paw), with a maximum score of 12 (3 score × 4 paws) per mouse. Change from baseline in

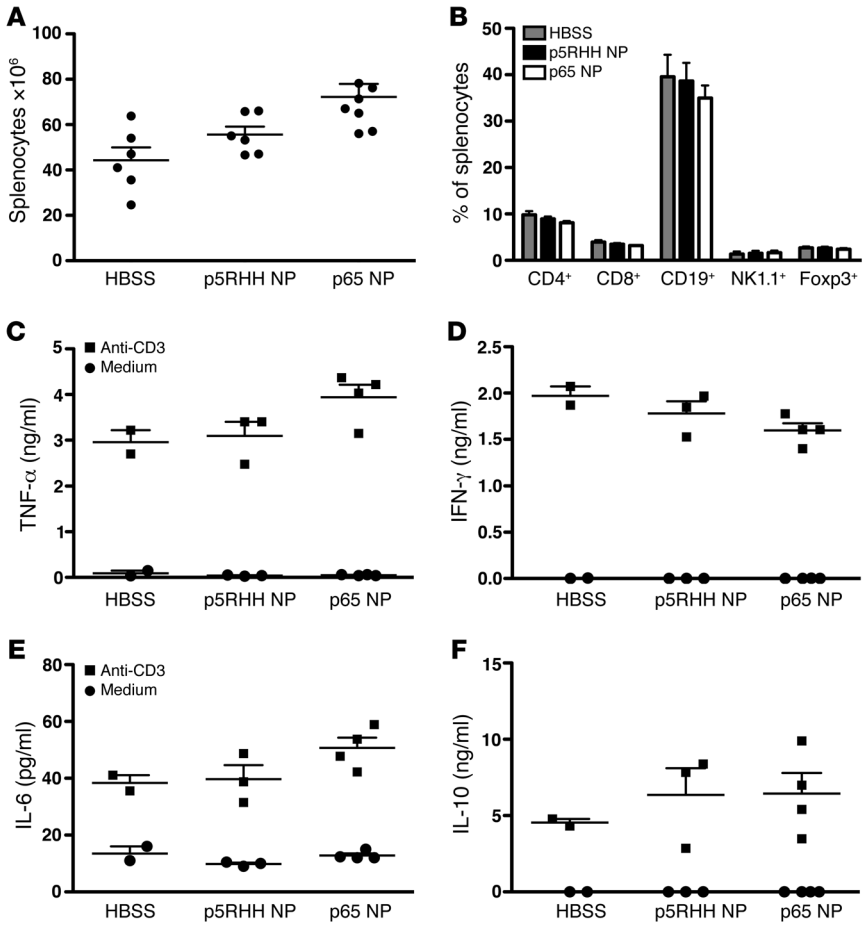

Figure 8. Effects of p5RHH-p65 siRNA nanoparticles on off-target immune cells. Arthritic mice were serially treated with HBSS, p5RHH siRNA nanoparticles, or p5RHH-p65 siRNA nanoparticles on days 4, 5, and 6, and spleens were harvested on day 10. (**A**) Splenocytes were enumerated upon harvest at day 10. (**B**) Splenic immune cell subpopulations were analyzed by flow cytometry using markers specific for T cells (CD4 and CD8), B cells (CD19), natural killer cells (NK1.1), and T regulatory cells (Foxp3). (**C**–**F**) Splenic $CD4^+$ T cells (2×10^5) were purified by magnetic beads and activated ex vivo on plate-bound anti-CD3 monoclonal antibody (5 μg/ml) for 72 hours. The supernatants were harvested and assayed for TNF-α (**C**), IFN-γ (**D**), IL-6 (**E**), and IL-10 (**F**) by cytometric bead array. $CD4^+$ T cells cultured in medium without anti-CD3 served as controls.

paw thickness was determined daily by dial calipers, and an average change in ankle thickness was determined for each mouse from the 2 hind paw measurements. Mice were also weighed every other day, and the percentage of weight loss from baseline was calculated. On day 10, mice were sacrificed, and their blood, paws, and organs were harvested for analysis.

Histologic analysis. Paws were harvested on day 10, fixed in 10% buffered formalin for 48 hours, decalcified in EDTA solution, embedded in paraffin, and sectioned at 5 μm. The sections were stained with H&E or toluidine blue. Inflammatory cell influx, bone erosions, and cartilage integrity were assessed as previously described (42, 43). Digital images of 5 random areas per H&E-stained paw section were acquired at ×400 magnification, and the number of exuded inflammatory cells was enumerated. The number of bone erosions was enumerated per millimeter of bone surface using ImageJ. Proteoglycan content, an indication of cartilage integrity, was graded on toluidine blue–stained sections on a scale of 0–4 (0, fully stained cartilage; 1, <25% unstained; 2, 25%–50% unstained; 3, 50%–75% unstained; 4, >75% unstained), as previously described (44). Quantitative scoring was performed by an observer blinded to the treatments. Each value represents the average per animal derived from the cumulative scoring of 2 hind paws.

Immunofluorescence. The frozen sections (9 μm) of harvested paws were fixed in 4% paraformaldehyde for 20 minutes at room temperature, incubated with rat anti-mouse F4/80 (1:100 dilution; catalog no. 14-4801, eBioscience), biotinylated rat anti-mouse Mac-3 (1:200 dilution; catalog no. CL8943AP, Cedarlane Laboratories), or rabbit anti-mouse p65 (1:100 dilution; catalog no. D14E12, Cell Signaling Technology), followed by incubation with the appropriate secondary antibody (1:100 dilution; Jackson Immunoresearch Laboratory). All images were visualized on a Nikon Eclipse microscope and acquired at the same exposure with QCapture software.

Real-time PCR. Total RNA from mouse paws was isolated using RNeasy Midi Kit (Qiagen Inc.) as recommended by the manufacturers. 2 μg RNA was used to synthesize cDNA by reverse transcription using the High Capacity cDNA Reverse Transcriptase kit (Applied Biosystems, Life Technologies) on a Multigene thermal cycler system (Labnet International Inc.). The reverse transcription product served as the template for real-time PCR analysis on a 7500 RT-PCR System (Applied Biosystems) using fluorogenic primers specific for p65 (PPM04224F, Qiagen Inc.), p100 (PPM03204G, Qiagen Inc.), and GAPDH (4352339E, Applied Biosystems) according to the manufacturer's recommendations. Total RNA recovered from p5RHH-p65 siRNA nanoparticle–treated mice was approximately 20-fold lower than controls due to the lack of inflammation/inflammatory cells. Data are presented as mRNA expression of target gene relative to *Gapdh*.

Western blot analysis. Ogran or paw lysates were prepared with 1% NP-40 lysis buffer containing proteinase inhibitor cocktail (Sigma-Aldrich). Briefly, cells or paws were homogenized, sonicated in the lysis buffer, and cleared by centrifugation at 18,000 *g* for 10 minutes at 4°C. Protein content was quantified and equivalent amount fractionated by SDS-PAGE under reducing conditions. Membranes were blotted with anti-p65, anti-p100/p52, anti-p105/p50, and anti-RelB

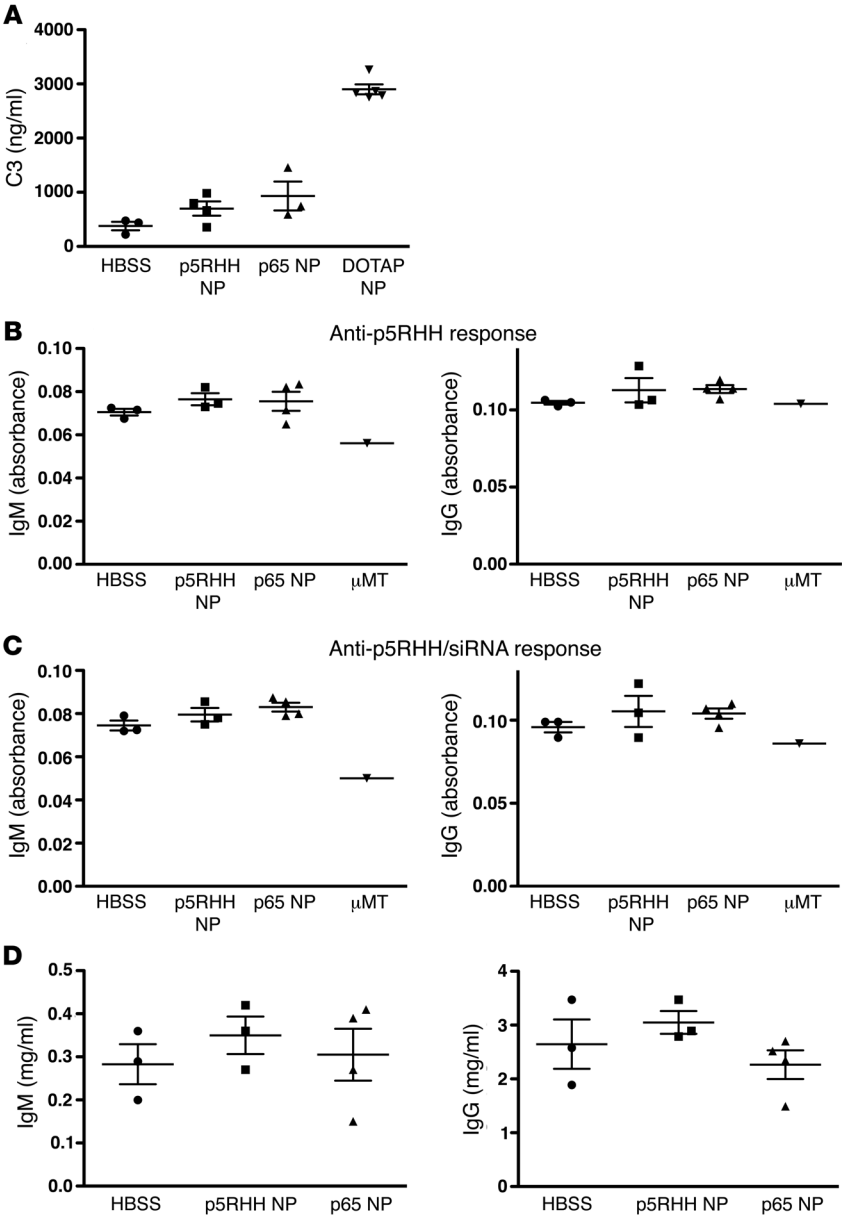

Figure 9. Effects of p5RHH-p65 siRNA nanoparticles on immune responses. (**A**) Naive mice were injected with 1 dose of HBSS, p5RHH siRNA nanoparticles, or p5RHH-p65 nanoparticles, and their plasma was obtained after 30 minutes for C3a assay as evidence of complement activation. Mice injected with 50 molar percentage of DOTAP (DOTAP NP) served as positive controls for robust complement activation. (**B** and **C**) Arthritic mice were serially treated with HBSS, p5RHH siRNA nanoparticles, or p5RHH-p65 siRNA nanoparticles on days 4, 5, and 6. On day 10, serum was obtained and probed for the presence of IgM and IgG antibodies against p5RHH (**B**) or the p5RHH siRNA nanocomplex (**C**). The levels of specific antibody response (measured by direct absorbance at 450 nm) were similar in all 3 treatment groups and minimally higher than the levels observed in μMT mice that lack all antibodies. (**D**) Total serum levels of IgM and IgG were also unchanged after nanoparticle treatment.

(1:1,000 dilution; catalog no. 4766S, Cell Signaling Technology) and anti-mouse β-actin (1:500 dilution; catalog no. sc-1615, Santa Cruz Biotechnology). The blots were washed and incubated with HRP-conjugated anti-rabbit IgG (1:2,000, Jackson ImmunoResearch Laboratories). Bands were visualized using a SuperSignal Western Blotting Kit (Thermo Scientific).

Cytokine analysis. Paws were homogenized in 1 ml PBS, and lysates were cleared by centrifugation. TNF-α, IL-6, and MCP-1 concentrations in paw lysates were measured by cytometric bead array using the Mouse Inflammation Kit (catalog no. 552364, BD Biosciences) according to the manufacturer's recommendations. IL-1β was measured by ELISA (R&D Systems) according to the manufacturer's recommendations.

Hematologic parameters and serum chemistries. Day 10 blood was drawn from the inferior vena cava and assayed for wbc counts/differentials and serum chemistries (hepatic and renal functions). Analysis was performed by the Washington University Department of Comparative Medicine.

Analysis of splenic subpopulations. Spleens were harvested and mechanically dissociated to obtain single-cell suspensions. The following antibodies were used: PE-conjugated anti-CD25 (PC61, BD Biosciences — Pharmingen), PE-conjugated anti-NK1.1 (PK136, eBioscience), FITC- or PerCP-conjugated anti-CD4 (L3T4, BD Biosciences — Pharmingen), FITC-conjugated anti-CD19 (1D3, BD Biosciences — Pharmingen), PerCP- or APC-conjugated anti-CD8 (53-6.7, BD Biosciences — Pharmingen). In general, 10^6 cells were blocked with the anti-FcR mAb 2.4G2, stained with the indicated Abs for 20 minutes at 4°C, and then washed and resuspended for FACS analysis. Foxp3 expression was analyzed using the Foxp3 Staining Kit (catalog no. 88-8118-40, eBioscience) according to the manufacturer's instructions. Flow cytometry was performed using a BD FACSCalibur. Data analysis was performed using BD CellQuest Pro software.

$CD4^+$ T cell purification and stimulation. $CD4^+$ T cells were isolated from mouse spleens with autoMACS Separator by positive magnetic sorting according to the manufacturer's protocol (MACS $CD4^+$ microbeads; catalog no. 130-049-201, Miltenyi Biotech). The purity of the isolated $CD4^+$ population was verified by surface staining with fluorescently labeled anti-CD4, anti-CD8, and anti-CD19 mAbs (BD Biosciences) and flow cytometry. Purified $CD4^+$ T cells were resuspended at 2×10^6 cells/ml in RPMI 1640 supplemented with 10% (v/v) FBS, 1% (v/v) NEAA, 1% (v/v) sodium pyruvate, 2 mM L-glutamine, 10 mM HEPES, 50 μM 2-mercaptoethanol, 100 μg/ml streptomycin, and 100 U/ml penicillin (Sigma-Aldrich), then plated at 2×10^5 cells/well in 96-well flat-bottomed microtiter plates coated with 5 μg/ml anti-CD3 mAb (BD Biosciences — Pharmingen) and cultured for 72 hours.

After the 72-hour incubation, culture supernatants were harvested, and cytokine concentrations were determined by BD Cytometric Bead Array (CBA) (Mouse Inflammation Kit; catalog no. 552364, BD Biosciences) according to the manufacturer's protocol. Cells were harvested and acquired on BD FACSCalibur for 45 seconds. Cell pro-

liferation was analyzed using BD CellQuest Pro software. All assays were performed in triplicate.

Immune responses to nanoparticles. Total IgG and IgM were measured using standard ELISA. Briefly, a 96-well plate was coated with goat anti-mouse IgG (Southern Biotechnology Associates Inc.) or goat anti-mouse IgM (Southern Biotechnology Associates Inc.) capture antibody (1 μg/ml in PBS) and incubated at 4°C overnight. After washing and blocking with 1% BSA in PBS, diluted mouse sera (1:40,00–1:400,00 dilution) were added to wells and incubated at room temperature for 1 hour. After further washing, 100 μl HRP-conjugated goat anti-mouse IgG (Southern Biotechnology Associates Inc.) or goat anti-mouse IgM (Southern Biotechnology Associates Inc.) antibody (1:3,000 dilution in 1% BSA in PBS) were added to the plate and incubated for 2 hours at room temperature. After washing, 100 μl peroxide-chromogen solution (R&D Systems) was added to each well, and color development was read at 450 nm with a SpectraMax Plus reader (Molecular Devices). Purified mouse IgG (Jackson ImmunoResearch Laboratories) and IgM (Rockland Immunochemicals) were used to establish the standard curves.

To measure IgM- or IgG-specific response to the p5RHH peptide or p5RHH siRNA nanocomplexes, 96-well plates (Immunlon 4 HBX; Thermo Fisher Scientific Inc.) were incubated with 100 μl/well of p5RHH peptide or p5RHH siRNA nanoparticles at a p5RHH peptide concentration of 2 μM at 4°C overnight. To determine the amount of material that bound to the surface of the wells, unbound p5RHH peptide or p5RHH siRNA nanoparticles were measured using a fluorescence spectrofluorometer (Varian Inc.). Since p5RHH contains 1 tryptophan residue, tryptophan fluorescence emission spectra (300–500 nm) were measured after excitation at 280 nm. Standard curves were generated, and the amounts of unbound materials were calculated against standard curves. For the p5RHH-coated plate, peptide was used at a concentration of 2.21 μg/ml. For the p5RHH siRNA–coated plate, the peptide was used at a concentration of 3.58 μg/ml. After washing and blocking with 1% BSA in PBS, diluted mouse sera (1:10–1:100 dilution) were added to wells and incubated for 1 hour at room temperature followed by HRP-conjugated goat anti-mouse IgG (Southern Biotechnology Associates Inc.) or goat anti-mouse IgM (Southern Biotechnology Associates Inc.) antibody as above. Color development was performed using peroxide-chromogen solution (R&D Systems) as above. Data are presented as direct absorbance (OD at 450 nm).

Off-target nanoparticle uptake. Mice were injected i.v. with 200 μl HBSS or Cy3-labeled peptide/scrambled RNA-seq nanoparticles. Mice were sacrificed after 30 minutes or 2 hours, and both peripheral blood wbcs and splenocytes were obtained at each time point for analysis of cell-associated Cy3-labeled particles by flow cytometry. Cells were also stained with Ly6G (neutrophils), Ly6C (monocytes), TCR-β (T cells), and CD19 (B cells) (all BD Biosciences — Pharmingen) to detect specific colocalization.

Complement activation. Mice were injected i.v. with 200 μl of peptide-siRNA nanoparticles. Blood was collected from the inferior vena cava at 30 minutes after nanoparticle injection directly into 10-mM EDTA tubes to prevent further ex vivo complement activation. Fresh plasma was prepared from collected blood for C3a ELISA. Briefly, plates were coated overnight at 4°C with rat anti-mouse C3a (4 μg/ml) monoclonal antibody (BD Biosciences). After blocking with reagent diluent (1% BSA in PBS) for 1 hour at RT, the plates were washed 3 times with ELISA wash buffer (0.05% [v/v] Tween 20 in PBS) and incubated with samples (100 μl of same-day, freshly obtained plasma diluted 1:100 in reagent diluent) for 1 hour at room temperature. Plates were washed 3 times, followed by incubation with biotinylated anti-mouse C3a (250 ng/ml) for 1 hour at room temperature. Plates were washed, incubated with streptavidin-peroxidase (400 ng/ml; Sigma-Aldrich) for 30 minutes, and washed again, after which 100 μl peroxide-chromogen solution (R&D Systems) was added to each well, and color development was read at 450 nm with a SpectraMax Plus reader (Molecular Devices). Mouse recombinant C3a (BD Biosciences) was used to establish the standard curve.

IVIS imaging. In vivo fluorescence images were acquired and analyzed with a Xenogen IVIS Spectrum imaging system (Caliper LifeSciences). During image acquisition, mice were maintained under isoflurane inhalation anesthesia. The settings (excitation, 640 nm; emission, 700 nm; exposure time, 2 s; binning factor, 8; f value, 2; field of view, 12.9) were used for image acquisitions at various time points after i.v. injection of nanoparticles containing Cy5.5 fluorophore–labeled scrambled siRNA, in free form or packaged in nanocomplexes. For the control animals, HBSS with Ca^{2+} and Mg^{2+} was injected i.v., and images were acquired using the same settings as above. The resultant pseudocolor "efficiency image" was used to illustrate the paw or organ accumulation of labeled siRNA.

Statistics. Comparisons between groups were performed by 2-tailed, unpaired *t* test without correction. Grading data were analyzed with χ^2 test. Comparisons among multiple groups (≥3) were performed by 1-way ANOVA. Equality of variance assumption was tested, and Bonferroni's correction for multiple comparisons was performed. Normality assumption appeared to be met, and tests for equality variance were conducted, revealing no differences. The sample size chosen (number of animals per treatment) was based on means and variances in similar experiments with various mouse models of arthritis for detection of differences between experimental groups at an α level of 0.05 and a statistical power of 0.80, assuming a 2-sided test.

Study approval. All animal experiments were performed in compliance with federal laws and in strict accordance with the guidelines established by the Division of Comparative Medicine at Washington University. The animal protocol is subjected to annual review and approval by The Animal Studies Committee of Washington University.

Acknowledgments

The authors thank Xiaoxia Yang for excellent technical assistance. This work was supported in part by NIH grants AI049261 and AR056468 and a bridge fund from the Dean and Department of Medicine at Washington University to C.T.N. Pham; a Sigma-Aldrich Predoctoral Fellowship to K.K. Hou; and NIH grants HL073646, HL112303, DK095555, and AR056223 and the James R. Hornsby Family Dream Garden Investment Partnership to S.A. Wickline. Histology included in this manuscript was performed by the Washington University Musculoskeletal Research Center, supported by NIH grant P30 AR057235.

Address correspondence to: Samuel A. Wickline, Division of Cardiology, Department of Medicine, Washington University School of Medicine, 660 South Euclid Avenue, Box 8215, Saint Louis, Missouri 63110, USA. Phone: 314.454.8811; E-mail: wicklines@aol.com. Or to: Christine T.N. Pham, Division of Rheumatology, Department of Medicine, Washington University School of Medicine, 660 South Euclid Avenue, Box 8045, Saint Louis, Missouri 63110, USA. Phone: 314.362.9043; E-mail: cpham@dom.wustl.edu.

1. Pasparakis M. Regulation of tissue homeostasis by NF-κB signalling: implications for inflammatory diseases. *Nat Rev Immunol*. 2009;9(11):778–788.
2. McInnes IB, Schett G. The pathogenesis of rheumatoid arthritis. *N Engl J Med*. 2011;365(23):2205–2219.
3. Szekanecz Z, Besenyei T, Paragh G, Koch AE. New insights in synovial angiogenesis. *Joint Bone Spine*. 2009;77(1):13–19.
4. Szekanecz Z, Besenyei T, Szentpetery A, Koch AE. Angiogenesis and vasculogenesis in rheumatoid arthritis. *Curr Opin Rheumatol*. 2010;22(3):299–306.
5. Agarwal SK. Biologic agents in rheumatoid arthritis: an update for managed care professionals. *J Manag Care Pharm*. 2011;17(9):S14–S18.
6. Buch MH, Bingham SJ, Bryer D, Emery P. Long-term infliximab treatment in rheumatoid arthritis: subsequent outcome of initial responders. *Rheumatology (Oxford)*. 2007;46(7):1153–1156.
7. Feist E, Burmester GR. Small molecules targeting JAKs--a new approach in the treatment of rheumatoid arthritis. *Rheumatology (Oxford)*. 2013;52(8):1352–1357.
8. Simmonds RE, Foxwell BM. Signalling, inflammation and arthritis: NF-κB and its relevance to arthritis and inflammation. *Rheumatology (Oxford)*. 2008;47(5):584–590.
9. Brown KD, Claudio E, Siebenlist U. The roles of the classical and alternative nuclear factor-kappaB pathways: potential implications for autoimmunity and rheumatoid arthritis. *Arthritis Res Ther*. 2008;10(4):212.
10. Criswell LA. Gene discovery in rheumatoid arthritis highlights the CD40/NF-κB signaling pathway in disease pathogenesis. *Immunol Rev*. 2010;233(1):55–61.
11. van Loo G, Beyaert R. Negative regulation of NF-kappaB and its involvement in rheumatoid arthritis. *Arthritis Res Ther*. 2011;13(3):221.
12. Hayden MS, Ghosh S. Shared principles in NF-κB signaling. *Cell*. 2008;132(3):344–362.
13. Hou KK, Pan H, Lanza GM, Wickline SA. Melittin derived peptides for nanoparticle based siRNA transfection. *Biomaterials*. 2013;34(12):3110–3119.
14. Hou KK, Pan H, Ratner L, Schlesinger PH, Wickline SA. Mechanisms of nanoparticle-mediated siRNA transfection by melittin-derived peptides. *ACS Nano*. 2013;7(10):8605–8615.
15. Sessa G, Freer JH, Colacicco G, Weissmann G. Interaction of alytic polypeptide, melittin, with lipid membrane systems. *J Biol Chem*. 1969;244(13):3575–3582.
16. Pan H, et al. Lipid membrane editing with peptide cargo linkers in cells and synthetic nanostructures. *FASEB J*. 2010;24(8):2928–2937.
17. Courtenay JS, Dallman MJ, Dayan AD, Martin A, Mosedale B. Immunisation against heterologous type II collagen induces arthritis in mice. *Nature*. 1980;283(5748):666–668.
18. Watson WC, Townes AS. Genetic susceptibility to murine collagen II autoimmune arthritis. Proposed relationship to the IgG2 autoantibody subclass response, complement C5, major histocompatibility complex (MHC) and non-MHC loci. *J Exp Med*. 1985;162(6):1878–1891.
19. Terato K, Hasty KA, Reife RA, Cremer MA, Kang AH, Stuart JM. Induction of arthritis with monoclonal antibodies to collagen. *J Immunol*. 1992;148(7):2103–2108.
20. Naeye B, et al. In vivo disassembly of IV administered siRNA matrix nanoparticles at the renal filtration barrier. *Biomaterials*. 2013;34(9):2350–2358.
21. Pham CT, et al. Variable antibody-dependent activation of complement by functionalized phospholipid nanoparticle surfaces. *J Biol Chem*. 2011;286(1):123–130.
22. Pham CT, et al. Application of a hemolysis assay for analysis of complement activation by perfluorocarbon nanoparticles. *Nanomedicine*. 2014;10(3):651–660.
23. Godl K, et al. An efficient proteomics method to identify the cellular targets of protein kinase inhibitors. *Proc Natl Acad Sci U S A*. 2003;100(26):15434–15439.
24. Davidson BL, McCray PB, McCray PB Jr. Current prospects for RNA interference-based therapies. *Nat Rev Genet*. 2011;12(5):329–340.
25. Schiffelers RM, Xu J, Storm G, Woodle MC, Scaria PV. Effects of treatment with small interfering RNA on joint inflammation in mice with collagen-induced arthritis. *Arthritis Rheum*. 2005;52(4):1314–1318.
26. Khoury M, et al. Efficient new cationic liposome formulation for systemic delivery of small interfering RNA silencing tumor necrosis factor alpha in experimental arthritis. *Arthritis Rheum*. 2006;54(6):1867–1877.
27. Khoury M, et al. Efficient suppression of murine arthritis by combined anticytokine small interfering RNA lipoplexes. *Arthritis Rheum*. 2008;58(8):2356–2367.
28. Zhang T, Bai X, Mao X. Systemic delivery of small interfering RNA targeting the interleukin-2/15 receptor β chain prevents disease progression in experimental arthritis. *PLoS One*. 2013;8(11):e78619.
29. Lee SJ, et al. TNF-α gene silencing using polymerized siRNA/thiolated glycol chitosan nanoparticles for rheumatoid arthritis. *Mol Ther*. 2014;22(2):397–408.
30. Duan J, et al. Polyethyleneimine-functionalized iron oxide nanoparticles for systemic siRNA delivery in experimental arthritis. *Nanomedicine (Lond)*. 2014;9(6):789–801.
31. Lv H, Zhang S, Wang B, Cui S, Yan J. Toxicity of cationic lipids and cationic polymers in gene delivery. *J Control Release*. 2006;114(1):100–109.
32. Soenen SJ, Brisson AR, De Cuyper M. Addressing the problem of cationic lipid-mediated toxicity: the magnetoliposome model. *Biomaterials*. 2009;30(22):3691–3701.
33. Whitehead KA, Langer R, Anderson DG. Knocking down barriers: advances in siRNA delivery. *Nat Rev Drug Discov*. 2009;8(2):129–138.
34. Plank C, Mechtler K, Szoka FC, Szoka FC Jr, Wagner E. Activation of the complement system by synthetic DNA complexes: a potential barrier for intravenous gene delivery. *Hum Gene Ther*. 1996;7(12):1437–1446.
35. Sevast'ianov VI, Tseytlina EA. The activation of the complement system by polymer materials and their blood compatibility. *J Biomed Mater Res*. 1984;18(9):969–978.
36. Moghimi SM, Andersen AJ, Ahmadvand D, Wibroe PP, Andresen TL, Hunter AC. Material properties in complement activation. *Adv Drug Deliv Rev*. 2011;63(12):1000–1007.
37. Pan H, et al. Postformulation peptide drug loading of nanostructures. *Methods Enzymol*. 2012;508:17–39.
38. Pan H, et al. Programmable nanoparticle functionalization for in vivo targeting. *FASEB J*. 2013;27(1):255–264.
39. Soman NR, Lanza GM, Heuser JM, Schlesinger PH, Wickline SA. Synthesis and characterization of stable fluorocarbon nanostructures as drug delivery vehicles for cytolytic peptides. *Nano Lett*. 2008;8(4):1131–1136.
40. Soman NR, et al. Molecularly targeted nanocarriers deliver the cytolytic peptide melittin specifically to tumor cells in mice, reducing tumor growth. *J Clin Invest*. 2009;119(9):2830–2842.
41. Leuschner F, et al. Therapeutic siRNA silencing in inflammatory monocytes in mice. *Nat Biotechnol*. 2011;29(11):1005–1010.
42. Zhou HF, Chan HW, Wickline SA, Lanza GM, Pham CT. Alphavbeta3-targeted nanotherapy suppresses inflammatory arthritis in mice. *FASEB J*. 2009;23(9):2978–2985.
43. Zhou HF, Hu G, Wickline SA, Lanza GM, Pham CT. Synergistic effect of antiangiogenic nanotherapy combined with methotrexate in the treatment of experimental inflammatory arthritis. *Nanomedicine (Lond)*. 2010;5(7):1065–1074.
44. Adkison AM, Raptis SZ, Kelley DG, Pham CT. Dipeptidyl peptidase I activates neutrophil-derived serine proteases and regulates the development of acute experimental arthritis. *J Clin Invest*. 2002;109(3):363–371.